



Soldering of diamond to molybdenum using a Zn–15Al alloy with semisolid phase assisted ultrasonic vibration

Takahisa Yamazaki¹ · Yutaro Ishii¹Received: 2 August 2019 / Accepted: 6 February 2020 / Published online: 10 February 2020
© Springer Nature Switzerland AG 2020

Abstract

Diamond was soldered to a molybdenum plate using a semisolid solder of Zn–15Al and ultrasonic vibration at brazing temperatures not exceeding 900 K. The joint interface was formed by a 10% aluminum solid phase in a semisolid solder when an ultrasonic vibration was applied to the interface. Several joints reached a shear strength of 40 MPa, although the shear strength results for the joints had a wide distribution. The Weibull plot of the strength test results revealed two categories of fracture interfaces. One category contained a flat diamond surface and a flat solder surface. The other category contained remaining solder on the diamond-joined surface. The first category had a shape that contained regions that were not joined. The second category reached a high joint strength over 40 MPa and had remaining solder on the fractured surface, a Weibull modulus $m = 1.5$ and a scale parameter $\eta = 52$ MPa. Adjacent to the joint interface, spherical alpha aluminum grains could be observed in the semisolid solder via applied ultrasonic vibration. Transmission electron microscopy was performed to observe the bonded interface of the diamond using the solder. The electron scattering images of the diamond that was cross sectioned with a focused ion beam revealed the formation of a few layers of crystallized alumina on the diamond interface. The alumina structure was spinel due to its formation at the low temperature of 900 K because zinc atoms were included in the layer. The reaction layer included carbon atoms that grew epitaxially from the diamond. The composition was considered to be $(\text{Zn}, \text{Al})_2(\text{O}=\text{C})_3$. It is hypothesized that ultrasonic vibration energy generates a reaction between the oxide on the diamond with the aluminum.

Keywords Ultrasonic soldering · Molybdenum · Semisolid · Diamond · Zinc–aluminum alloy

1 Introduction

Diamond has excellent properties of hardness, compressive strength, electric insulation, and chemical stability [1]. Diamond is a quasi-stable structure of carbon at high temperature, so soldering at 900 K in an inert atmosphere can damage diamond. Using infrared radiation heating in a vacuum, the surface of diamond decomposes by molecular vibrations, desorbing carbon dioxide gas and hydrocarbons from the surface [2–4]. Soldering diamonds under 723 K in air is necessary for many applications.

Zinc–aluminum (Zn–Al) alloys have low melting temperatures that are below 723 K. A Zn–14 at.% Al solder (near the eutectic point of Zn–11.3 at.% Al) was used to join an aluminum alloy to a carbon steel at 663 K with different ultrasonic vibration times. When carbon steel was brazed using a Zn–Al solder, applying an ultrasonic vibration for 3 s allowed the formation of Fe_3Al , which improved the joint bond strength. In addition, the formation of Fe–Al compounds after 4 s of ultrasonication decreased the joint bond strength, but the strength remained above that obtained without ultrasonic vibration [5].

✉ Takahisa Yamazaki, yamazaki.t.ae@m.titech.ac.jp; Yutaro Ishii, caanaanc@gmail.com | ¹School of Engineering, Tokyo Institute of Technology, Tokyo 152-8550, Japan.



Ultrasonic soldering creates a cavitation effect, which removes bubbles and oxide films from the metal surface and promotes wetting of the solder. The Zn–Al solder did not wet the diamond surface with a rosin flux during soldering [4]. When an ultrasonic melt treatment was applied, grain refinement occurred in an aluminum alloy containing Zr and Ti. The refinement of the grains was related to the formation of Al₃Zr particles as the primary crystals [6]. Using a Zn–14 mass% Al hypereutectic filler metal, an ultrasonically brazed aluminum alloy was produced. The spherically shaped primary alpha aluminum phase in the molten brazing filler caused grain refinement as a result of the ultrasonic vibration [7]. An interface of aluminum–diamond composite materials was investigated, and the Al–diamond interface was generally clean except for the formation of reaction products. In the procedure for producing the aluminum–diamond composite, ultrasonic vibration was not applied. However, an interfacial amorphous disordered carbon layer was observed, and aluminum carbide phase Al₄C₃ was formed [8]. We attempted to use Zn–15 mass% Al with the primary Al phase to solder the diamond with a clean interface.

The mechanism of joining 10% solid-phase aluminum using semisolid solder and applied an ultrasonic vibration is still unclear [9]. Transmission Electron Microscope

equipped with Energy Dispersed Spectroscopy (TEM/EDS) work was carried out to observe the interface of the diamond with the solder joint.

2 Materials and methods

Molybdenum was selected as the base metal plate due to the small thermal expansion ratio and ability to ultrasonically solder using Zn–15Al. The solder (Akita Zinc Solutions) had a liquidus line at 724 K. An artificial diamond (SUMICRYSTAL by Sumitomo Electric Industries, Ltd.), type IB, was cleaved and polished along the (111) plane. The dimensions of the diamond were 1.4 × 1.4 × 1.1 mm. The joint specimens for the strength test were manufactured via ultrasonic soldering at 60 kHz and 15 W with a stainless steel tip that had a diameter of 4 mm (using SUNBONDER USM-IV Kuroda Techno Co. Ltd.). The dimensions of the molybdenum plate (Nilaco Cooperation) were 50 × 10 × 0.8 mm.

The times that the ultrasonic vibration was applied are presented in Table 1. An extended ultrasonication time was required for the diamond on the molybdenum base plate to be wet by the molten solder because the wetting of the solder on the diamond was poorer than that on the

Table 1 Joining conditions and shear strength test results

Specimen No.	Step 1 Preliminary soldering of Mo plate [3 s] Temperature [K]	Step 2 Preliminary soldering of diamond [15 s] Temperature [K]	Step 3 Soldering of diamond to Mo plate [3 s] Temperature [K]	Shear strength [MPa]	Number <i>i</i>
1	593 (No ultrasonic)	Skip step 2	723	5.51	1
2	593 (No ultrasonic)	Skip step 2	723	8.00	2
3	593 (No ultrasonic)	Skip step 2	723	8.31	3
4	593 (No ultrasonic)	Skip step 2	723	14.4	8
5	593 (No ultrasonic)	Skip step 2	723	14.9	10
6	623	723	723	8.53	4
7	623	723	723	11.2	5
8	623	723	723	12.1	6
9	623	723	723	12.8	7
10	623	723	723	14.4	8
11	623	723	723	19.3	11
12	623	723	723	20.1	12
13	623	723	723	21.6	13
14	623	723	723	22.5	14
15	623	723	723	35.6	15
16	623	723	723	36.1	16
17	623	723	723	37.5	17
18	623	723	723	47.4	18
19	623	723	723	49.7	19
20	623	723	723	64.8	21
21	723	723	723	61.8	20

Fig. 1 Three steps in the ultrasonic soldering of a diamond to a Mo plate

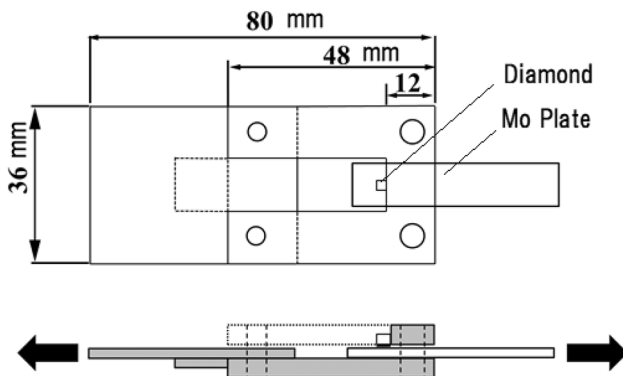
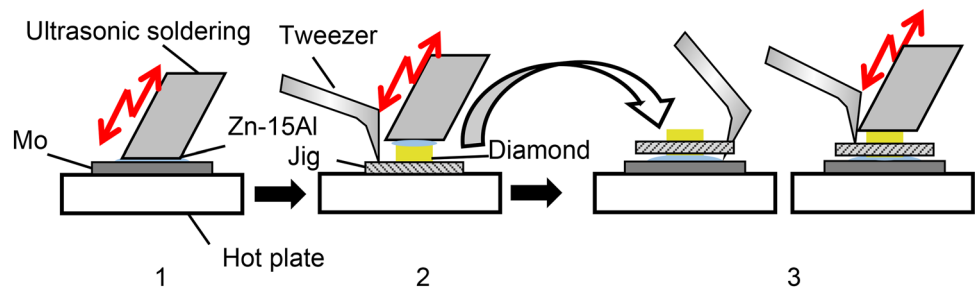


Fig. 2 Shear test jig for the diamond joint sample for a tensile load

molybdenum base plate. The soldering conditions are presented in Table 1. The molybdenum plate was preheated at 623 K, and then molten Zn–15Al solder was applied with an ultrasonic vibration by a stainless steel tip at 723 K (step 1), as shown in Fig. 1. The ultrasonication time for wetting the plate required was 3 s [6, 7].

The Zn–15Al solder foil was first mounted onto the diamond surface, and an ultrasonic lateral wave vibration at a tip angle of 66° was applied to the molten solder (step 2). The ultrasonication time required for wetting the diamond in step 2 was 15 s. The preheating temperature of the diamond was 723 K.

Finally, using tweezers, we mated the solder layer on the diamond to that on the plate. An ultrasonic vibration was then applied to form the joint (step 3) for the short time of 3 s. To produce a well-aligned diamond joint for the strength test, an additive jig was used as a clip with tweezers, as shown in Fig. 1.

The joint strength was evaluated by shear strength testing using the adaptive jig for the tensile test as shown in Fig. 2. The u-shaped part, which was made of a steel plate of 5 mm thick, came in contact with the diamond side to apply the load. The clearance between the u-shaped jig and a Mo plate was adjusted using a plate of 36 mm wide. The holes were produced to fix the u-shape jig and the plate using bolts and nuts. The adaptive jig was clamped by the chuck on the tensile testing machine (LSC-02/30



Fig. 3 Joint specimen comprising diamond soldered to a Mo plate

Tokyo Koki Testing Machine Co. Ltd. The cross-head speed was varied from 1 to 30 mm/min). The long molybdenum plate was clamped by the bottom chuck of the tensile testing machine. The cross-head speed was set to the slowest speed available, which was 1 mm/min. One strength test specimen was produced using the clip for the diamond, as shown in Fig. 3.

2.1 Analysis

The shear strength data for the soldered joints, which had a wide distribution, were analyzed by a Weibull plot. The plot was expressed by the following function:

$$F(x) = 1 - \exp \left\{ - \left(\frac{x}{\eta} \right)^m \right\} \quad (1)$$

where m is the Weibull modulus (shape parameter), x expresses shear stress, and η is the normalizing stress (scale parameter). For example, using a binominal distribution of the data, the shape parameter of the plot was calculated to be 2 from the Weibull plot analysis. Another

example, when the data are fit with a Rayleigh distribution, the shape parameter is 2 in the Weibull distribution.

When there are abundant data, the fracture probability function F should be calculated from $F = (i - 0.3)/(n + 0.4)$, which is the median rank method, where n is the total sample number and i is the numbering in the median rank method via x . In this paper, the number of joined diamond samples was limited as 21, so the fracture probability function with the mean rank method is $F = i/(n + 1)$, which is usually used for less than 21 samples. There were several fractured samples at the same shear strength, so the values of F differed from each other, and the Weibull plot data of $\ln(\ln(1/1 - F))$ diverged from the linear line via $\ln x$.

3 Results

The Weibull probability plot of the shear strength for the soldered joint is shown in Fig. 4. The total number n of strength test specimens for the plot was 21. The joint conditions and shear strength are presented in Table 2. The three fractured specimens below 10 MPa did not contain preliminary diamond soldering and were out of the range of the collected joint data because the data were plotted from 10 to 30 MPa. Different slopes for the strength are shown by this plot for the area beyond 30 MPa. There were specimens with strong joint interfaces among the tested samples.

The plots under 30 MPa showed a linear relationship with $m = 1.74$ and scale parameter $\eta = 22.5$ MPa. By screening the plotted data, m was estimated to be 1.5 for the 7 data points over 30 MPa, and the scale parameter became $\eta = 52$ MPa, although two data points were obtained by fracturing at a high cross-head speed before decreasing to a slow speed. The difference in the strength among

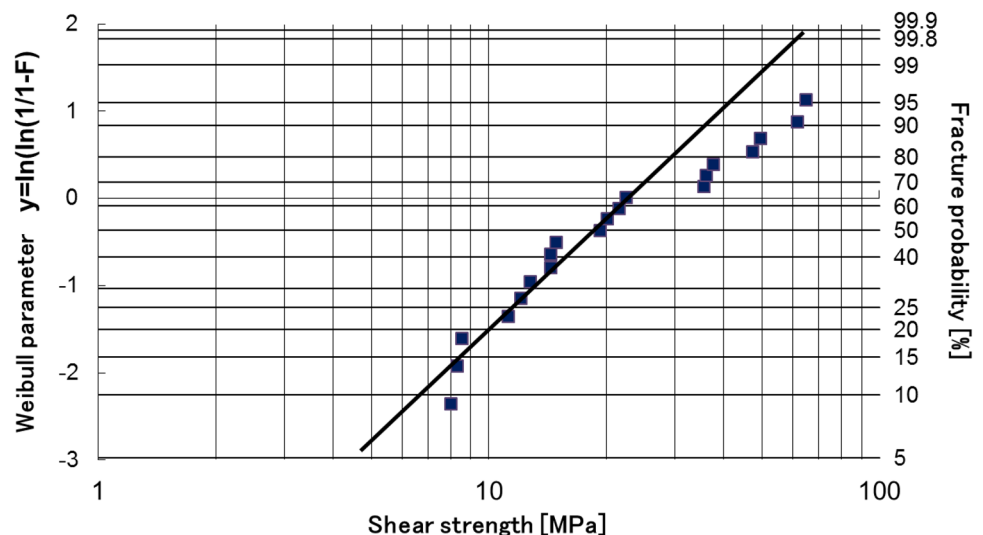
Table 2 Compositions at the points analyzed with TEM/EDS in Fig. 8

Position	Zn (at.%)	Al (at.%)	O (at.%)	C (at.%)
1	95.945	1.909	1.146	0
2	15.73	42.66	41.61	0
3	1.053	39.82	31.15	27.98
4	0.863	0.325	0.604	98.21

the joints was due to the bonding interface produced by the ultrasonic vibration of the remaining Zn–15Al solder on the fractured surface of the diamond. The joint specimens fractured under 18 MPa, unless the diamond was preliminarily soldered. The interface between the diamond and Zn–15Al solder with an applied ultrasonic vibration plays an important role in the strong bonding. The plotted screening data showed a linear relationship, indicating that the interface was brittle.

Figure 5 shows the TEM/EDS sample fabricated by FIB (focused ion beam) for the solder adhered on the diamond with a (111) surface after the shear strength test (the shear strength was 64.8 MPa). Figure 6 shows the interfacial TEM image of the diamond. Carbon, aluminum and zinc elements were detected by EDS analyses. The carbon atomic layers of the diamond lattice can be observed in the TEM image. The layer adjacent to the diamond is alumina, which had an ordered lattice. The structure of the alumina is considered to be spinel according to the pattern [9–11]. The [220] direction is indicated by the arrow. The electron diffraction patterns of the No. 1 and No. 2 areas in Fig. 6 are shown in Fig. 7. The aluminum crystal reciprocal lattice cannot be observed in Fig. 7 (No. 1 area), although the aluminum layers on the right side of the lattice can be observed. Amorphous aluminum atoms are deposited on the spinel alumina layer with atomic layer thicknesses. In

Fig. 4 Weibull plot of the shear strength of the soldered diamond samples



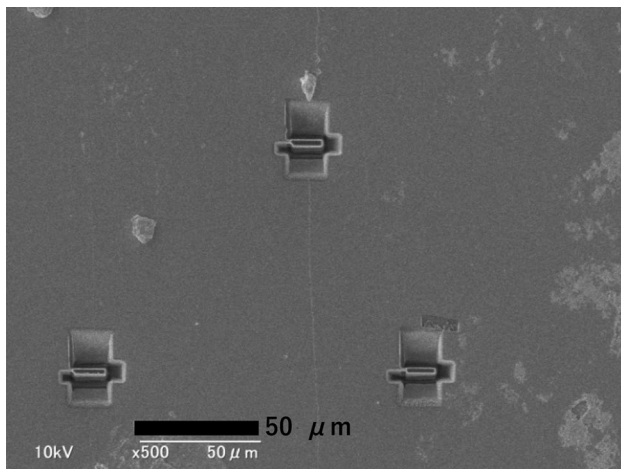


Fig. 5 FIB fabrication of TEM samples of adhered solder on diamond (111)

the No. 2 position, a zinc HCP (hexagonal close packed) reciprocal lattice pattern can be obtained; thus, zinc atoms were deposited on amorphous aluminum atoms upon

Fig. 6 Diamond/Solder interface observed by TEM and the high-resolution image at interface No.1

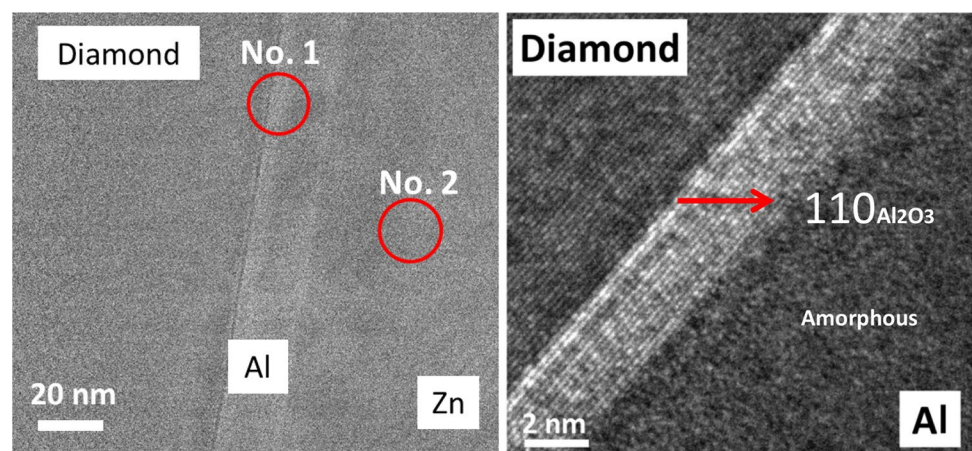
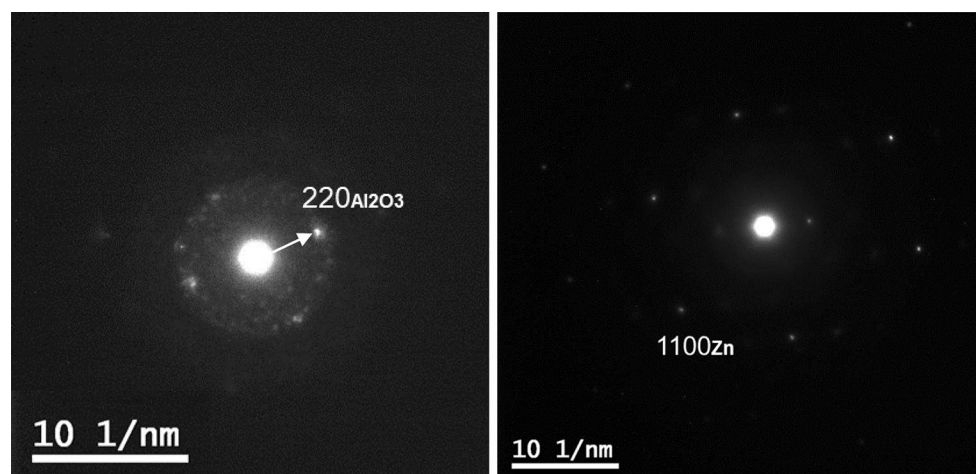


Fig. 7 Electron diffraction images of the No. 1 and No. 2 positions in Fig. 6



solidification in the last step of soldering, and the direction of deposition was considered to be [0001] due to the reciprocal lattice 1100 that was observed (irradiation direction was considered to be [0001]).

The TEM/EDS results revealed the formation of gamma alumina at the diamond interface. The EDS spot analysis results are presented in Table 2, and the points used for the analysis spots are shown in Fig. 8. In spot 3, aluminum atoms included zinc atoms in a given ratio, as well as oxygen and carbon atoms, so the final ratio became 2:3. This result is indicative of the formation of alumina: $(Zn, Al)_2(O=C)_3$, although the formation of $ZnAl_2O_4$ reported previously [11], was not detected. The atomic ratio of aluminum and carbon was almost 4:3 and considered to be related to Al_4C_3 formation. The interface formation of $(Zn, Al)_2(O=C)_3$ generated the joint strength between the diamond crystal and the Zn–15Al solder. In spot 2, the percentage of aluminum atoms was 42.66 at.%, the thickness of the aluminum layer in Fig. 6 was 20 nm, and the electron diffraction pattern rings of the face-centered cubic (FCC) aluminum structure were obtained. This layer was considered to be formed along the aluminum solidus line

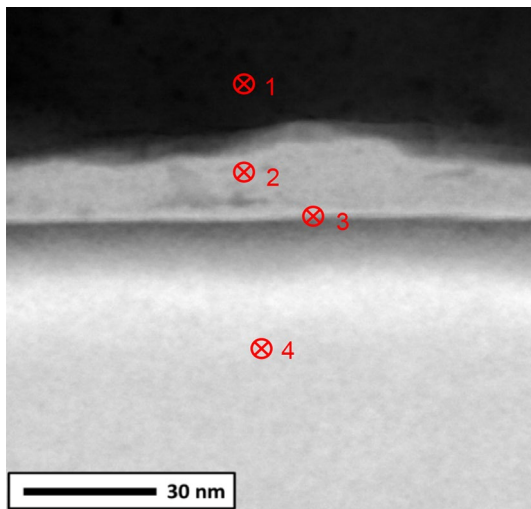


Fig. 8 TEM/EDS image of the soldered interface

including zinc, within the temperature range of the semi-solid phase of the solder. In spot 1 in Fig. 8, zinc atoms are detected. This spot was near the No. 1 electron diffraction pattern obtained in Fig. 6. The deposition of zinc atoms occurred on metal aluminum oriented to the FCC structure of aluminum during the solidification of the Zn–15Al solder at the eutectic point of 654 K at the last step of soldering; thus, the amount of Al atoms was limited.

4 Discussion

In previous works using a semisolid solder of the Zn–Al system, the diamond could be joined to a molybdenum plate using an ultrasonic solder tip, and the joint strength had a wide distribution from 7 MPa to 58 MPa. In the case of 90% liquid phase solders of various compositions in the Zn–Al system, the diamond could be stably joined to a molybdenum plate. The joint made by Zn–15Al solder had a shear strength of 40 MPa. The X-ray diffraction pattern showed a Zn (0002) peak and Al (111) peak for the soldered diamond with (111) in Fig. 9. A peak representative of Al (111) peak was observed at 38.450° in the diffraction pattern obtained using Cu K α radiation; in addition a peak for Al (200) appeared at 44.6°, and Al (220) was obtained at 65.1° in 2 θ [12]. In this study, only the Al (111) peak was observed. The X-ray diffraction patterns for aluminum and zinc in Fig. 9 were identified, although we assumed the formation of Al₄C₃ would strengthen the solder. Although the characteristic peak of Al₄C₃ appears at 43.5°, no peaks for Al₄C₃ were detected. In addition, no graphite peaks were observed. When the diamond was heated under atmospheric conditions at 770 K, it reacted with oxygen to allow oxidation of the diamond with graphitization of

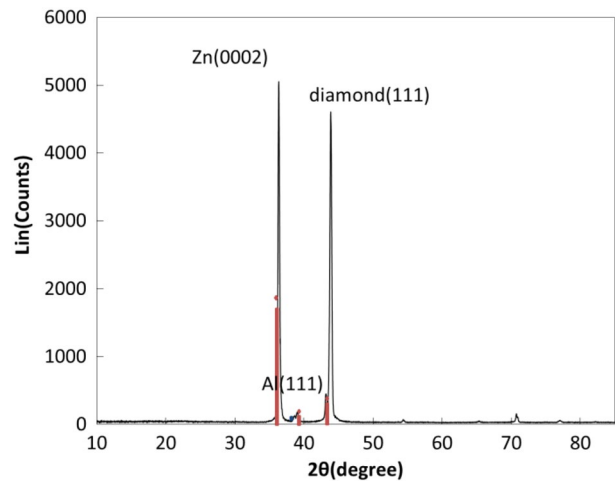


Fig. 9 X-ray diffraction pattern of the diamond surface prepared via ultrasonic soldering using Zn–15Al solder

the surface. Thus, the diamond soldered at 723 K was not considered graphitized. The formation of (Zn, Al)₂(O=C)₃ on the diamond (111) surface was confirmed by TEM of the high-strength joints in this work. The layer was oriented to the diamond surface. A thin aluminum layer comprising primary aluminum spherical particles played an important role in the strengthening of joints. TEM revealed the formation of aluminum oxide [13], which was considered to be a gamma phase alumina at lower temperatures, including 720 K. Gamma alumina is spinel structure, so in [11] ZnAl₂O₄ is supposed to resemble MgAl₂O₄ [14].

Primary fine aluminum crystals were dispersed by ultrasonic vibration in the molten solder at soldering step 2, and the aluminum crystal removed oxygen atoms from the diamond surface as well as from the molybdenum base plate at soldering step 1; therefore, aluminum atoms can be detected in the lamella near the surfaces and as round shapes in the solder. The grain size of the primary crystal of aluminum was 0.5 μ m, and the round aluminum grain in the solder was 10 μ m. According to the TEM observation in Fig. 6, amorphous aluminum deposited on the lamella alumina formed at the soldering step 2 when ultrasonic vibration was applied with a duration of 15 s.

The diffraction pattern revealed a peak shift of zinc toward low angles, indicating enlargement of the lattice space toward Zn (0100) and narrowing toward Zn (0002). The Zn (0002) peak was larger than the Zn (1010) peak at a 2 θ value of 38.9°, as shown in Fig. 10. The relations between the Zn peaks based on the X-ray analysis revealed that the distortion of the Zn crystal lattice a-axis was larger than that of the c-axis. The lattice constant of the a-axis was 0.2672 nm, although it is ideally 0.2665 nm, and the c-axis had a lattice constant of 0.4949 nm rather than the ideal value of 0.4946 nm [12]. The interface between the

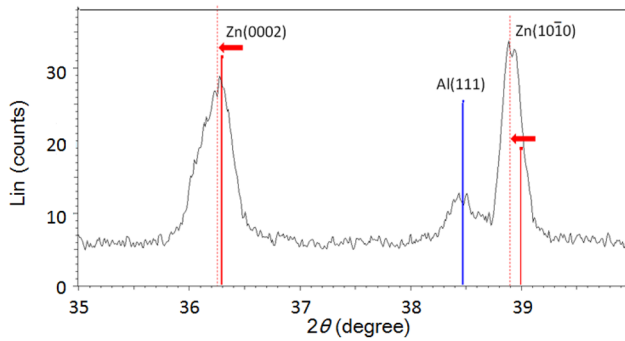


Fig. 10 X-ray diffraction pattern of the diamond surface prepared via ultrasonic soldering using Zn–15Al solder around Al(111)

amorphous aluminum layer and hetero epitaxial zinc layer was considered brittle because delamination and deformation of the TEM observation specimens was observed in Fig. 5 was observed. The hetero epitaxial zinc layer was considered to be formed in the solidification process in the last step, step 3.

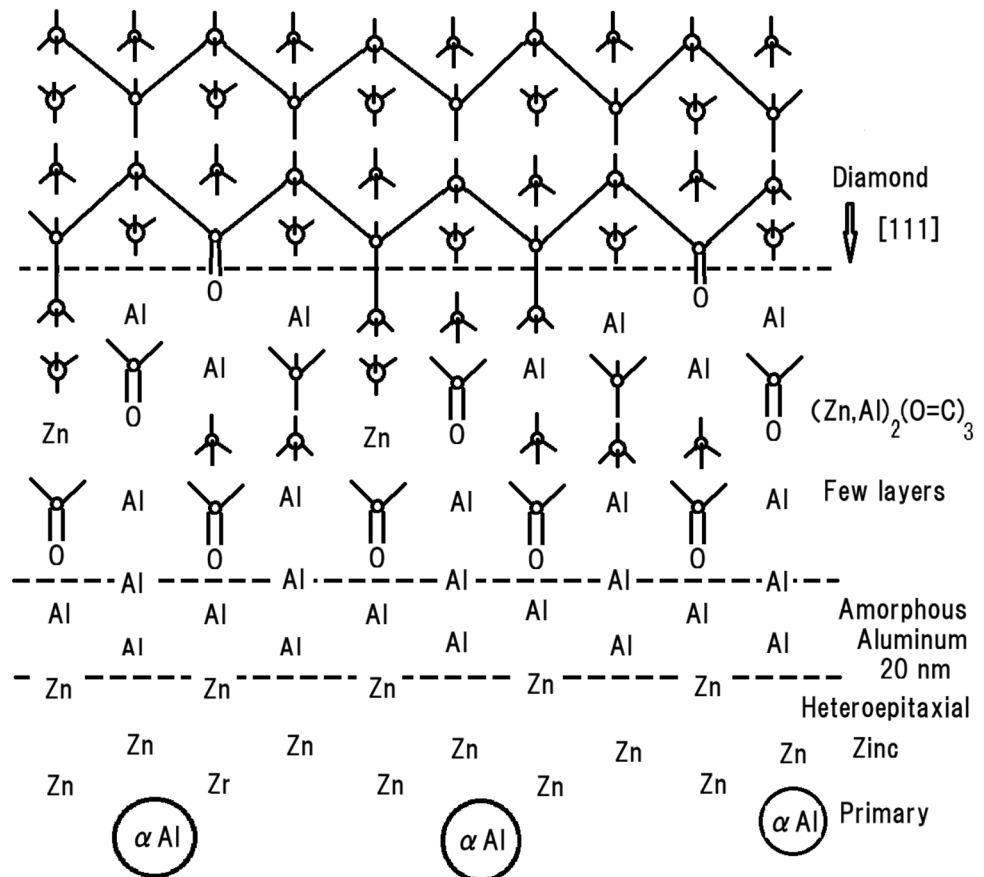
Figure 11 shows an illustration of a joint interface from a diamond (111) formed by using Zn–15Al semisolid solder assisted ultrasonic vibration. The primary aluminum crystal in the solder reached the diamond surface, and the

oxidized carbons were broken by the vibration. The broken carbon oxide molecules $(C=O)^{2-}$ and aluminum ions Al^{3+} including zinc atoms formed spinel structure of alumina. The broken carbon atoms were considered to form aluminum carbide. Metal aluminum atoms adhered to the oxygen atoms of $C=O$ and were deposited amorphously, followed by progression of the deposition of aluminum. When the molten solder solidified, heterogeneous nucleation of zinc (0002) occurred from the deposited aluminum surface. The round primary spherical aluminum grains were distributed in the solidified solder. The hetero epitaxial interface between zinc and aluminum generated stress related to the lattice dislocation based on the X-ray diffraction pattern. The brittle interface has a high fracture strength and wide distribution of stress.

5 Conclusions

The fracture strength was measured using well-aligned diamond joint specimens soldered by Zn–15Al that was assisted by ultrasonic vibration. The Weibull plot for the shear strength of the soldered diamond to the molybdenum plate shows different slopes for the joints with a high strength. The group that had the remaining Zn–15Al

Fig. 11 Schematic illustration of the interface with (111) diamond using Zn–15Al semi-solid solder and an applied ultrasonic vibration



solder on the diamond surface in the fracture test also had a linear fracture probability function with the logarithm of shear strength after screening the Weibull plot data. The Weibull modulus was 1.5, and the shape parameter was 52 MPa. The Weibull modulus did not reach 3 for the Gaussian distribution; thus, the joints had brittle interfaces. These specimens were observed by TEM/EDS. The interface cross-section between the diamond and the adhered Zn–15Al solder was produced with FIB. The observation revealed the formation of a spinel structure of alumina that was oriented with the diamond. The alumina contained carbon atoms related to the formation of Al_4C_3 and zinc atoms in the structure of spinel. In the soldering process herein that was assisted by ultrasonic vibration, aluminum primary crystals in the solder cleaned the oxidized surface on the diamond and molybdenum plate without a halogen atom flux. The cleaning of the oxidized surfaces on the diamond and molybdenum plate by the primary crystals of aluminum and formation of the spinel alumina generated the sound joint interface. This approach holds promise as a joining process for carbon materials and metals.

Acknowledgements Analyses using X-ray diffraction were supported by the National University Corporation Tokyo Institute of Technology Center for Advanced Materials Analysis. The TEM and STEM work was supported by the Suzukakedai Analysis Center in Tokyo TECH.

Author contributions TY designed the study, analyzed data and wrote the manuscript. YI performed the experiments and made the figures.

Compliance with ethical standards

Conflict of interest The authors have no conflicts of interest to declare.

References

1. Novikov NV (1987) Physical property of diamond. Ohm Printing in Japan, Hamamatsu
2. Sakaguchi S, Yamazaki T, Ikeshoji T-T, Suzumura A (2011) Quadrupole mass spectrometer analysis of pyrolysis gases from

3. diamond with through lamp heat for joining to metal ring. Preprints of the National Meeting of J.W.S., vol 89, pp 302–303
3. Pehrsson PE, Mercer TW (2000) Oxidation of the hydrogenated diamond (100) surface. *Surf Sci* 460:49–66
4. Yamazaki T, Tsuda H, Sakaguchi S, Ikeshoji T-T, Suzumura A (2013) Reaction product between diamond and manganese powder heated by condensed infrared rays for metallization. In: 10th international conference. German Welding Society, DVS, Aachen, pp 283–286
5. El-Sayed MH, Naka M (2005) Structure and properties of carbon steel-aluminum dissimilar joints. *Sci Technol Weld Join* 10:27–31
6. Atamanenko TV, Eskin DG, Zhang L, Katgerman L (2010) Criteria of grain refinement induced by ultrasonic melt treatment of aluminum alloys containing Zr and Ti. *Metall Mater Trans A* 41A:2056–2066. <https://doi.org/10.1007/s11661-010-0232-4>
7. Xiao Yong, Ji Hongjun, Li Mingyu, Kim Jongmyung, Kim Hona-bae (2013) Microstructure and joint properties of ultrasonically brazed Al alloy joints using a Zn–Al hypereutectic filler metal. *Mater Des* 47:717–724. <https://doi.org/10.1016/j.matdes.2013.01.004>
8. Khalid FA, Beffort O, Klotz UE, Keller BA, Gasser P (2004) Microstructure and interfacial characteristics of aluminum–diamond composite materials. *Diam Relat Mater* 13:393–400. [https://doi.org/10.1016/S0925-9635\(03\)00567-3](https://doi.org/10.1016/S0925-9635(03)00567-3)
9. Susukida K, Tada K, Yamazaki T (2016) Soldering of diamond using Zn–15Al solder by applying ultrasonic vibration. In: LÖT, international conference brazing, high temperature brazing and diffusion bonding, 11Verlag für Schweißen und verwandte Verfahren, DVS-Verlag, Aachen, pp 372–377
10. Ishimaru M (2017) Transmission electron microscopy studies on radiation-induced structural changes. *Kenbikyō* 52–1:24–28
11. Zerarga F, Bouhemadou A, Khenata R, Bin-Omran S (2011) Structural, electronic and optical properties of spinel oxides $ZnAl_2O_4$, $ZnGa_2O_4$ and $ZnIn_2O_4$. *Solid State Sci* 13:1638–1648
12. JSPDS-International Centre for Diffraction Data
13. Dominguez D, Tiznado H, Borbon-Nuñez HA, Muñoz-Muñoz F, Romo-Herrera JM, Soto G (2016) Enhancing the oxidation resistance of diamond powder by the application of Al_2O_3 conformal coat by atomic layer deposition. *Diam Relat Mater* 69:108–113
14. Castro RHR, Ushakov SV, Gengembre L, Gouvêa D, Navrotsky A (2006) Surface energy and thermodynamic stability of γ -alumina: effect of dopants and water. *Chem Mater* 18:1867–1872

Publisher's Note Springer Nature remains neutral with regard to jurisdictional claims in published maps and institutional affiliations.